Multivariable Grid-Forming Converters With Direct States Control

Chen, Meng; Zhou, Dao; Blaabjerg, Frede

Published in:
I E E E Transactions on Industry Applications

DOI (link to publication from Publisher):
10.1109/TIA.2023.3269021

Publication date:
2023

Document Version
Accepted author manuscript, peer reviewed version

Multivariable Grid-Forming Converters with Direct States Control

Meng Chen, *Member, IEEE,* Dao Zhou, *Senior Member, IEEE,* and Frede Blaabjerg, *Fellow, IEEE*

***Abstract*—This paper presents an improved multi-input multi-output based grid-forming (MIMO-GFM) converter control method using multivariable feedback control. Although the original MIMO-GFM control is proven to be superior and robust using only low-order controllers, it is easily affected by high-frequency components, particularly for the converter without inner cascaded voltage and current loops and when it is connected into a strong grid. The proposed method selects frequency and internal voltage as state variables to be directly controlled while effectively eliminating the impact of high-frequency components without increasing system complexity. The $\mathcal{H}_\infty$ synthesis is used to tune the parameters to obtain an optimized performance. Experimental results and system-level simulations verify the effectiveness of the proposed method.**

***Index Terms*—multi-input multi-output grid-forming (MIMO-GFM), direct states control, $\mathcal{H}_\infty$ synthesis, power converter, loops coupling.**

I. Introduction

THE integration of inverter-interfaced generators (IIGs) has become a vital aspect of modern power systems due to growing concerns about environmental issues and fossil fuel consumption [1], [2]. Grid-following control is commonly used in systems with low penetration of IIGs, where the stability is maintained by synchronizing with the conventional synchronous generator-dominated system, e.g., through a phase-locked loop (PLL) [3]. With the rapid increase in the penetration of IIGs, the ability of self-establishment of the frequency and voltage without relying on external power sources is supposed as essential for some of the IIGs in the future, particularly in systems with 100% IIGs [4]. In this regard, grid-forming control presents a promising solution [5], [6].

Up to now, several basic grid-forming controls have been widely researched, e.g., droop control [7], [8], virtual synchronous generator (VSG) control [9]–[11], power synchronization control [12], matching control [13], etc. All of them are proposed based on various assumptions of loops decoupling such as AC power and DC voltage loops, active and reactive power loops. In other words, they try to treat the grid-forming converter as several decoupled single-input single-output (SISO) systems [9], [10]. These assumptions simplify the analysis but, at the same time, may sacrifice the performance. Therefore, although the aforementioned grid-forming controls can basically achieve the frequency and voltage regulation, they may not be superior and robust to different operation conditions. To improve the performance of the basic grid-forming controls, several kinds of their improved forms have been proposed, which are usually with higher-order controllers and more complicated control structures to deal with each loops [14], [15].

Recently, a new perspective from the multi-input multi-output (MIMO) system to construct and design the grid-forming control has been proposed [16], [17]. In this way, the coupling information among different loops can be used to improve the performance with simple control structures. In [17], the fundamental theory has been studied using a multivariable feedback control in detail, where a control transfer matrix is used to deal with all the AC power and DC voltage loops as a MIMO integrity and unify different kinds of grid-forming controllers. Thereafter, a MIMO based grid-forming (MIMO-GFM) controller is proposed, which can provide a superior and robust performance without increasing the order of the system. Nevertheless, due to the coupling between the AC power and DC voltage loops, the frequency and internal voltage of the MIMO-GFM converter is sensitive to the high-frequency components of the error signals, which is inevitable. This is because the frequency and internal voltage are not direct state variables. The influence will be more obvious when the grid-forming converter is connected to a strong grid without cascaded voltage and current loops. In this case, in practice, pre-filters for decreasing the high-frequency disturbances are necessary.

It should be mentioned that such pre-filters are very common in other control strategies, e.g., the power filters in the droop control [18] and the DC voltage filter in the matching control [19]. As the pre-filters are not related to the principle of the control strategies, they are sometimes neglected during the analysis in some literature, which is not preferable. Take the droop control as an example, it has been revealed that the system is hard to be stable for some systems without the power filters, which is due to the lack of enough inertia of the pure droop control [20]. Moreover, it is also proven that the droop control with power filters is equivalent to the VSG control to some extent, which will not be found if neglecting the power filters [21]. In summary, the pre-filters may, on the one hand, lead to mismatch between the theoretical analysis and the practical results, and on the other hand, increase the order and complexity of the system [22].

Motivated from the aforementioned analysis, this paper extends the work in [17]. First, the reason why the original MIMO-GFM control is high-frequency sensitive is analyzed from the point view of the state-space. Thereafter, a new form of control transfer matrix is proposed. The coupling

This work was supported by the Reliable Power Electronic-Based Power System (REPEPS) project at the Department of Energy Technology, Aalborg University as part of the Villum Investigator Program funded by the Villum Foundation.

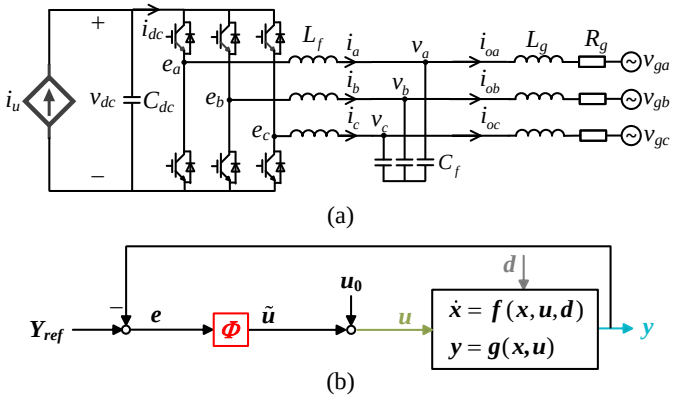

Fig. 1. Grid-forming converter. (a) Topology. (b) Equivalent closed-loop multivariable feedback control configuration.

information can still be used to provide a superior and robust performance. Meanwhile, the frequency and internal voltage are chosen as state variables to be controlled [1]. As a result, the impact of the high-frequency components on the frequency and internal voltage is suppressed without relying on the pre-filters and thus without increasing the complexity of the control system.

The rest of this paper is organized as follows. In Section II, the preliminaries on MIMO-GFM control is introduced, where its problem is also analyzed in this section. The proposed control and design are given in Section III. In Section IV, experimental results and system-level simulation are presented, and finally, conclusions are drawn in Section V.

II. Preliminary of MIMO-GFM Converters and Problem Definition

A. Basic Principle of MIMO-GFM Converters

Fig. 1 shows the studied topology of the grid-forming converter and its equivalent MIMO closed-loop feedback control configuration. A typical three-phase voltage source inverter is connected to the power grid via an LC filter and a grid line, where L_f and C_f are the inductance and capacitance of the LC filter, L_g and R_g are the equivalent inductance and resistance of the grid line. If an LCL filter is used, the grid-side inductance can be considered into L_g. The DC source is represented by a controlled-current source i_u paralleled with a DC capacitor, where the capacitance is C_{dc}.

Then the state-space model of the topology can be built in the d-q frame and it is represented in a compact form in Fig. 1(b) as

$$\dot{\boldsymbol{x}} = \boldsymbol{f}(\boldsymbol{x},\boldsymbol{u},\boldsymbol{d}) \tag{1}$$

$$\boldsymbol{y} = \boldsymbol{g}(\boldsymbol{x},\boldsymbol{u}) \tag{2}$$

and the vectors are defined as

$$\boldsymbol{x} = \begin{bmatrix} i_d & i_q & v_d & v_q & i_{od} & i_{oq} & \delta & v_{dc} \end{bmatrix}^T \tag{3}$$

$$\boldsymbol{u} = \begin{bmatrix} i_u & \omega_u & E_u \end{bmatrix}^T \tag{4}$$

$$\boldsymbol{y} = \begin{bmatrix} v_{dc} & p & \omega_u & q & V \end{bmatrix}^T \tag{5}$$

$$\boldsymbol{d} = \begin{bmatrix} \omega_g & V_g \end{bmatrix}^T, \tag{6}$$

where i_{dq} are the currents of the filter inductor, v_{dq} are voltages of the filter capacitor, i_{odq} are the output currents, δ is the angle difference between the grid-forming converter internal voltage and the grid voltage, v_{dc} is the DC voltage, ω_u and E_u are the frequency and internal voltage to be obtained by the grid-forming controller, p and q are the output active and reactive powers, respectively, V is the magnitude of the capacitor voltage, ω_g and V_g are the frequency and magnitude of the grid voltage. Moreover, the detailed mathematical model of the system can be given as

$$\dot{i}_d = \frac{\omega_b}{L_f}E_u - \frac{\omega_b}{L_f}v_d + \omega_b\omega_u i_q \tag{7}$$

$$\dot{i}_q = -\frac{\omega_b}{L_f}v_q - \omega_b\omega_u i_d \tag{8}$$

$$\dot{v}_d = \frac{\omega_b}{C_f}i_d - \frac{\omega_b}{C_f}i_{od} + \omega_b\omega_u v_q \tag{9}$$

$$\dot{v}_q = \frac{\omega_b}{C_f}i_q - \frac{\omega_b}{C_f}i_{oq} - \omega_b\omega_u v_d \tag{10}$$

$$\dot{i}_{od} = \frac{\omega_b}{L_g}v_d - \frac{\omega_b}{L_g}V_g\cos\delta - \frac{\omega_b R_g}{L_g}i_{od} + \omega_b\omega_u i_{oq} \tag{11}$$

$$\dot{i}_{oq} = \frac{\omega_b}{L_g}v_q + \frac{\omega_b}{L_g}V_g\sin\delta - \frac{\omega_b R_g}{L_g}i_{oq} - \omega_b\omega_u i_{od} \tag{12}$$

$$\dot{\delta} = \omega_b\omega_u - \omega_b\omega_g \tag{13}$$

$$\dot{v}_{dc} = \frac{\omega_b}{C_{dc}}i_u - \frac{\omega_b E_u i_d}{C_{dc}v_{dc}} \tag{14}$$

$$p = v_d i_{od} + v_q i_{oq} \tag{15}$$

$$q = -v_d i_{oq} + v_q i_{od} \tag{16}$$

$$V = \sqrt{v_d^2 + v_q^2} \tag{17}$$

As observed, the DC dynamics, active power dynamics, and reactive power dynamics are coupled with each other. Although most of the researches assume that those dynamics are decoupled during the closed-loop design, they are not decoupled exactly. The coupling information could provide extra freedom to improve the performance of the system. Motivated from this point, in Fig. 1(b), $\boldsymbol{\Phi}(s) = (\phi_{ij})_{3\times 5}$ is a control transfer matrix, which copes with all the loops as a MIMO integrity rather than decoupled SISO systems. In [17], $\boldsymbol{\Phi}$ is designed as follows for the MIMO-GFM converter

$$\boldsymbol{\Phi}_{MIMO} = \begin{bmatrix} k_{pdc} + \frac{k_{idc}}{s} & k_{12} & 0 & k_{14} & k_{15} \\ k_{21} & D_p k_{22}/(s+k_{22}) & 0 & k_{24} & \frac{k_{24}}{D_q} \\ k_{31} & k_{32} & 0 & k_{34}/s & \frac{k_{34}/D_q}{s} \end{bmatrix} \tag{18}$$

where D_p and D_q are the droop coefficients for active and reactive power controls, respectively. As shown, the MIMO-GFM controller keeps all the favorable features of the basic controllers, i.e., inertia and droop characteristics. Meanwhile, it uses several simple proportional gains to deal with the coupling terms, which has been proved as an effective way to provide a superior and robust performance without increasing the order of the system.

B. Impact of High-Frequency Components

To better illustrate the problem of the MIMO-GFM controller, we will first consider a basic VSG control. The control

transfer matrix Φ can be derived by setting all the coupling gains of (18) as zero

$$\boldsymbol{\Phi}_{VSG} = \begin{bmatrix} k_{pdc}+k_{idc}/s & 0 & 0 & 0 & 0 \\ 0 & D_p k_{22}/(s+k_{22}) & 0 & 0 & 0 \\ 0 & 0 & 0 & k_{34}/s & \frac{k_{34}/D_q}{s} \end{bmatrix} \tag{19}$$

based on which the state differential equations of Φ_{VSG} can be expressed as

$$\dot{x}_{\phi VSG1} = k_{idc} e_1 \tag{20}$$

$$\dot{x}_{\phi VSG2} = -k_{22} x_{\phi VSG2} + D_p k_{22} e_2 \tag{21}$$

$$\dot{x}_{\phi VSG3} = k_{34} e_4 + \frac{k_{34}}{D_q} e_5 \tag{22}$$

and the state variables are defined as

$$\boldsymbol{x}_{\phi VSG} = \begin{bmatrix} \tilde{i}_u - k_{pdc} e_1 & \tilde{\omega}_u & \tilde{E}_u \end{bmatrix}^T \tag{23}$$

Similarly, the state differential equations of Φ_{MIMO} in (18) can be expressed as

$$\dot{x}_{\phi MIMO1} = k_{idc} e_1 \tag{24}$$

$$\dot{x}_{\phi MIMO2} = -k_{22} x_{\phi MIMO2} + D_p k_{22} e_2 \tag{25}$$

$$\dot{x}_{\phi MIMO3} = k_{34} e_4 + \frac{k_{34}}{D_q} e_5 \tag{26}$$

and the state variables are defined as

$$\boldsymbol{x}_{\phi MIMO} = \begin{bmatrix} \tilde{i}_u - k_{pdc} e_1 - k_{12} e_2 - k_{14} e_4 - k_{15} e_5 \\ \tilde{\omega}_u - k_{21} e_1 - k_{24} e_4 - \frac{k_{24}}{D_q} e_5 \\ \tilde{E}_u - k_{31} e_1 - k_{32} e_2 \end{bmatrix} \tag{27}$$

The following conclusions can be summarized.

1) From (20)-(23), the control of the basic VSG is decoupled, i.e., $\tilde{i}_u$ is controlled by e_1, $\tilde{\omega}_u$ is controlled by e_2, $\tilde{E}_u$ is controlled by e_4 and e_5.
2) Comparing (20)-(22) with (24)-(26), it is observed that the state differential equations of the VSG and MIMO-GFM controls have the same structure.
3) Comparing (23) with (27), the state variables between the VSG and MIMO-GFM controls are quite differnt.

Therefore, it is clear that the principle of the MIMO-GFM control is to change the state variables by adding the coupling terms but not to change the form of the state differential equations compared with the basic VSG control. These coupling terms are expected to improve the performance because they provide a multi-degree-of-freedom control and the useful coupling information among various loops can be considered as well.

Nevertheless, due to the changes of the state variables, the frequency $\tilde{\omega}_u$ and internal voltage $\tilde{E}_u$ are not the state variables to be directly controlled anymore for the MIMO-GFM converter. Instead, they will be directly influenced by the errors $\boldsymbol{e}$ as shown in (27), especially the high-frequency components, which are inevitable. On one hand, there are always high-frequency components in the steady-state powers and DC voltage. On the other hand, steps of the references $\boldsymbol{Y}_{ref}$ will also introduce the high-frequency components into the errors. Therefore, in practice, pre-filters are usually used before

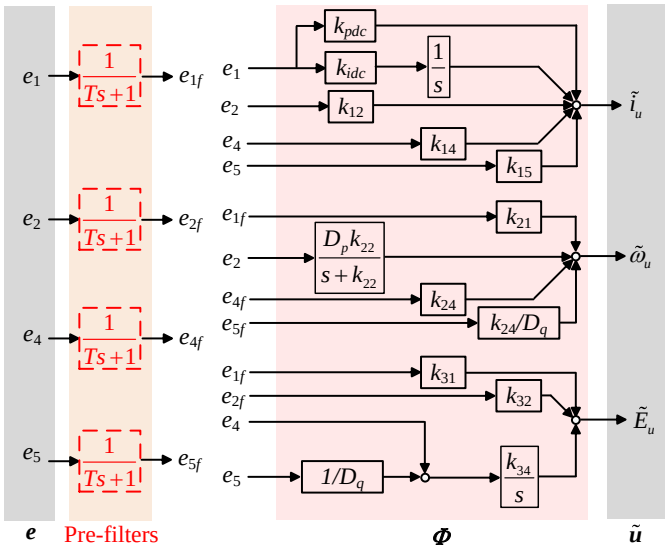

Fig. 2. Practical control block diagram of MIMO-GFM converter with pre-filters.

the coupling terms in order to suppress the influence of the high-frequency components as shown in Fig. 2. However, these pre-filters increase the order and complexity of the system and may highly influence the stability.

III. Proposed Direct States Control

A. Principle of Proposed Direct States Control

According to the aforementioned analysis, the problem of the MIMO-GFM control is due to the fact that the added coupling terms change the state variables compared with the basic VSG control. Motivated from this point, an improved MIMO-GFM control is proposed, where the state differential equations of the control transfer matrix is designed as

$$\dot{x}_{\phi 1} = -k_{12} x_{\phi 2} + k_{idc} e_1 + D_p k_{12} e_2 + k_{14} e_4 + \frac{k_{14}}{D_q} e_5 \tag{28}$$

$$\dot{x}_{\phi 2} = -k_{22} x_{\phi 2} + k_{21} e_1 + D_p k_{22} e_2 + k_{24} e_4 + \frac{k_{24}}{D_q} e_5 \tag{29}$$

$$\dot{x}_{\phi 3} = -k_{32} x_{\phi 2} + k_{31} e_1 + D_p k_{32} e_2 + k_{34} e_4 + \frac{k_{34}}{D_q} e_5 \tag{30}$$

and the state variables are defined as

$$\boldsymbol{x}_{\phi} = \begin{bmatrix} \tilde{i}_u - k_{pdc} e_1 & \tilde{\omega}_u & \tilde{E}_u \end{bmatrix}^T \tag{31}$$

The following conclusions about the proposed control can be summarized.

1) Comparing (31) with (23), the proposed control chooses the same state variables as the basic VSG control. Especially, the frequency and internal voltage are still directly controlled state variables.
2) Comparing (28)-(30) with (20)-(22) and (24)-(26), it is observed that the state differential equations of the proposed control has a different structure, which is taking the coupling terms into consideration.

In this way, the proposed control can not only suppress the influence of the high-frequency components but also

improve the performance using the coupling terms. It should also be mentioned, from (28)-(30), that the proposed method still hold the steady-state droop characteristics. Therefore, the steady-state operation points will be automatically determined through the defined droop characteristics when multiple inverters are paralleled. The corresponding control transfer matrix of the proposed method can be derived as

$$\boldsymbol{\Phi}(s) = (\phi_{ij})_{3\times 5} \tag{32}$$

where

$$\phi_{11} = \frac{k_{pdc}s^2 + (k_{pdc}k_{22} + k_{idc})s + k_{idc}k_{22} - k_{12}k_{21}}{s^2 + k_{22}s} \tag{33}$$

$$\phi_{12} = \frac{D_p k_{12}}{s + k_{22}},\ \phi_{14} = \frac{k_{14}s + k_{14}k_{22} - k_{12}k_{24}}{s^2 + k_{22}s} \tag{34}$$

$$\phi_{15} = \frac{(k_{14}/D_q)s + k_{14}k_{22}/D_q - k_{12}k_{24}/D_q}{s^2 + k_{22}s} \tag{35}$$

$$\phi_{21} = \frac{k_{21}}{s + k_{22}},\ \phi_{22} = \frac{D_p k_{22}}{s + k_{22}} \tag{36}$$

$$\phi_{24} = \frac{k_{24}}{s + k_{22}},\ \phi_{25} = \frac{k_{24}/D_q}{s + k_{22}} \tag{37}$$

$$\phi_{31} = \frac{k_{31}s + k_{22}k_{31} - k_{21}k_{32}}{s^2 + k_{22}s},\ \phi_{32} = \frac{D_p k_{32}}{s + k_{22}} \tag{38}$$

$$\phi_{34} = \frac{k_{34}s + k_{22}k_{34} - k_{24}k_{32}}{s^2 + k_{22}s} \tag{39}$$

$$\phi_{35} = \frac{(k_{34}/D_q)s + k_{22}k_{34}/D_q - k_{24}k_{32}/D_q}{s^2 + k_{22}s} \tag{40}$$

$$\phi_{13} = \phi_{23} = \phi_{33} = 0 \tag{41}$$

According to the aforementioned analysis, the block diagram of the proposed control transfer matrix is as shown in Fig. 3. It is worth mentioning that although the above elements of ϕ_{ij} seem to have complicated forms, according to (28)-(31), the order of the system is not increased and the control structure is straightforward as well, which is because ϕ_{ij} actually share many common parts as shown in Fig. 3. As observed, it still only uses simple proportional controllers to include the coupling terms. After obtaining $\tilde{\omega}_u$, the angle of the power converter voltage can be derived as

$$\theta = \int_0^t (1 + \tilde{\omega}_u)\omega_b d\tau \tag{42}$$

where θ is used for all the transformations between d-q frame and abc frame.

B. Parameters Design based on $\mathcal{H}_\infty$ Optimization

To make a fair comparison with the original MIMO-GFM control, this paper also uses the $\mathcal{H}_\infty$ synthesis to tune the parameters to obtain an optimal performance [17]. Therefore, the block diagram of the proposed control transfer matrix in Fig. 3 is equivalently changed to Fig. 4 by defining two intermediate vectors $\hat{\boldsymbol{u}}$ and $\hat{\boldsymbol{y}}$, which have the following relationship

$$\begin{aligned}\hat{\boldsymbol{u}} &= diag(k_{pdc}, k_{idc}, k_{21}, k_{31}, k_{12}\boldsymbol{I_2}, k_{22}\boldsymbol{I_2}, k_{32}\boldsymbol{I_2}, k_{14}, k_{24}, k_{34})\hat{\boldsymbol{y}} \\ &= \boldsymbol{K}\hat{\boldsymbol{y}}\end{aligned} \tag{43}$$

where $\boldsymbol{K}$ is a gain vector only containing all the parameters to be tuned. Thereafter, the standard form of linear fractional

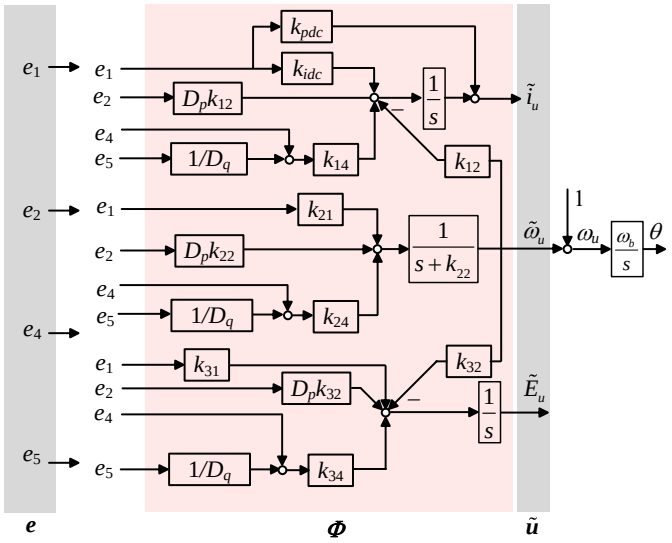

Fig. 3. Block diagram of proposed control transfer matrix Φ.

transformation for $\mathcal{H}_\infty$ optimization can be obtained as shown in Fig. 5, where the grid-forming converter in Fig. 1(b) is collapsed into $\mathbf{G}$ (except for $\boldsymbol{K}$). The disturbance inputs and evaluation outputs for the $\mathcal{H}_\infty$ synthesis are defined as

$$\boldsymbol{w} = \begin{bmatrix} P_{ref} & \omega_g \end{bmatrix}^T \tag{44}$$

$$\boldsymbol{z} = \begin{bmatrix} P_{ref} - p & p & \omega_u & q + V/D_q \end{bmatrix}^T \tag{45}$$

where the transfer functions from w_j to z_i is denoted as $T_{ij}(s)$. For example, $T_{21}(s)$ is the transfer function from $w_1 = P_{ref}$ to $z_2 = p$. These transfer functions are limited by the following chosen weighting functions $W_{ij}(s)$

$$W_{11}(s) = \frac{s+4}{s+0.0004} \tag{46}$$

$$W_{21}(s) = \left(\frac{1.447\times 10^{-3}s + 1}{1.447\times 10^{-5}s + 1}\right)^2 \tag{47}$$

$$W_{22}(s) = \frac{1}{100} \times \frac{1.447\times 10^{-3}s + 1}{1.447\times 10^{-5}s + 1} \tag{48}$$

$$W_{31}(s) = \frac{1}{0.015} \times \frac{s}{1.447\times 10^{-5}s + 1} \tag{49}$$

$$W_{32}(s) = \frac{1.447\times 10^{-3}s + 1}{1.447\times 10^{-5}s + 1} \tag{50}$$

$$W_{41} = \frac{s+60}{s+0.006} \tag{51}$$

and the considerations of choosing the weighting functions can be found in [17]. Finally, the parameters can be derived by solving the following $\mathcal{H}_\infty$ optimization problem

$$\min_{\boldsymbol{K}} ||diag(W_{ij}(s)T_{ij}(s))||_\infty \tag{52}$$

According to the aforementioned method with the parameters listed in Table I, the parameters of the proposed control can be derived as shown in Table II. As an example, Fig. 6 presents the log magnitude curves of the designed transfer function $T_{21}(s)$ from P_{ref} to p and its weighting function $W_{21}(s)$. As observed, by solving (52), $T_{21}(s)$ is limited by $W_{21}^{-1}(s)$. Therefore, the high-frequency suppression of $T_{21}(s)$

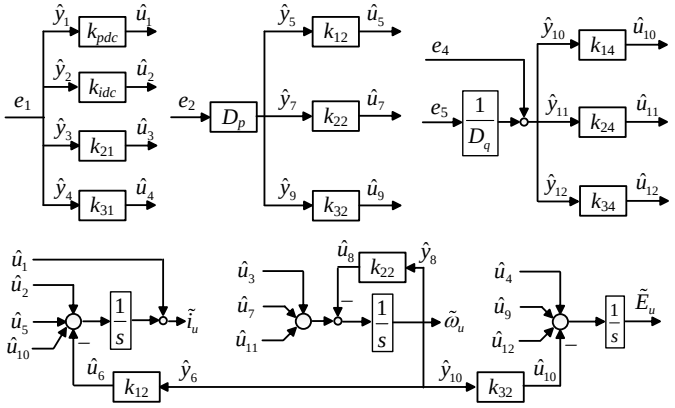

Fig. 4. Equivalent block diagram of proposed control transfer matrix for the formulation of $\mathcal{H}_\infty$ synthesis.

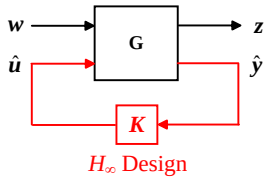

Fig. 5. Block diagram of grid-forming converter in linear fractional transformation.

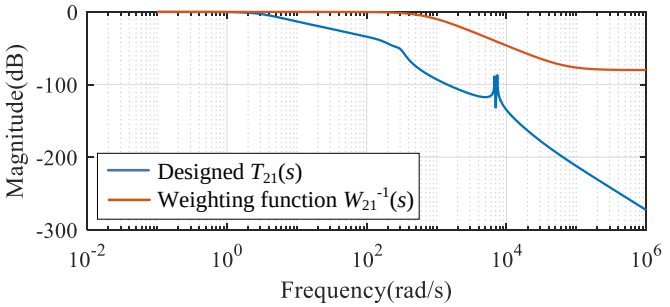

Fig. 6. Log magnitude curves of designed transfer function $T_{21}(s)$ and its weighting function $W_{21}(s)$.

can be guaranteed by properly choosing $W_{21}(s)$. Other transfer functions as well as their corresponding weighting functions are similar. For the following comparison, the parameters of the original MIMO-GFM control are also presented in Table II. Supposing there is a disturbance in e_1, Fig. 7 compares the bode diagrams of the closed-loop transfer function from this disturbance to ω_u. The advantage of considering a disturbance in e_1 compared to a disturbance in reference is that both the disturbances in the reference and the feedback channel can be included. As observed, the original MIMO-GFM control without those pre-filters fails to suppress the components with the frequency over 200 rad/s. In comparison, the proposed control make the log-magnitude curve to decrease with a slope of -40 dB/decade even though we have neither defined an explicit weighting function to limit the corresponding high-frequency components nor added any pre-filter, which verify the advantages of the proposed control method.

TABLE I
PARAMETERS OF TEST SYSTEM

Symbol	Description	Value
ω_n	nominal frequency	100π rad/s
S_n	nominal power	4 kW
V_n	nominal line-to-line RMS voltage	380 V
f_{sw}	switching frequency	10 kHz
ω_g	grid frequency	100π rad/s (1 p.u.)
V_g	grid voltage	380 V (1 p.u.)
L_g	line inductor	2 mH (0.0174 p.u.)
R_g	filter resistor	0.06 Ω (0.0017 p.u.)
C_f	filter capacitor	20 μF (0.2268 p.u.)
L_f	filter inductor	2 mH (0.0174 p.u.)
R_f	filter resistor	0.06 Ω (0.0017 p.u.)
C_{dc}	DC capacitor	500 μF (19.2423 p.u.)
D_p	droop coefficient of P-f regulation	0.01 p.u.
D_q	droop coefficient of Q-V regulation	0.05 p.u.
P_{ref}	Active power reference	0.5 p.u.
Q_{ref}	Reactive power reference	0 p.u.
V_{ref}	Voltage magnitude reference	1 p.u.
V_{dcref}	DC voltage reference	700 V

TABLE II
PARAMETERS OF CONTROL TRANSFER MATRIX FOR ORIGINAL MIMO-GFM AND PROPOSED CONTROLLERS

Parameters	Original MIMO-GFM Control	Proposed Control
k_{pdc}	120.224	18.8801
k_{idc}	265.6217	2811.2
k_{12}	-0.0019	123.7138
k_{14}	0.1673	4.9404
k_{15}	-0.8274	-
k_{21}	-0.8382	-20.1083
k_{22}	1.7622	0.5532
k_{24}	0	0.0615
k_{31}	-4.8977	5.684
k_{32}	0	-0.1862
k_{34}	1.0844	0.0908

IV. EXPERIMENTAL RESULTS AND SYSTEM-LEVEL SIMULATION VALIDATION

A. Experimental Results

The performance of the proposed control is tested by using the experimental setup shown in Fig. 8. The parameters are the same as those in Table I and Table II, which represents a system of a grid-forming converter connected to a strong grid. The structure of the control system is same as Fig. 1 without cascaded voltage and current loops. Meanwhile, due to the DC control is fixed in the DC source, only the power loops can be tested. Nevertheless, it does not influence the conclusion.

Fig. 9 compares the experimental results with the original MIMO-GFM control and the proposed control when P_{ref} steps from 0.5 p.u. to 1 p.u. It should be mentioned that no any pre-filter is included in the control system. As shown, although the original MIMO-GFM control can guarantee the stability

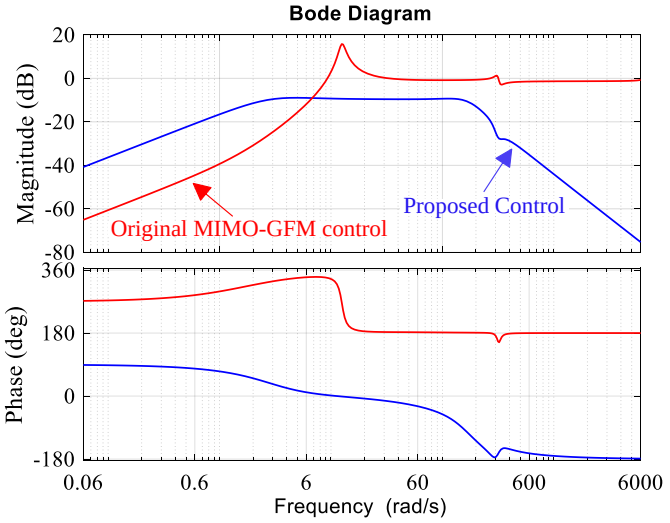

Fig. 7. Comparison of bode diagram between original MIMO-GFM control and proposed control without any pre-filter.

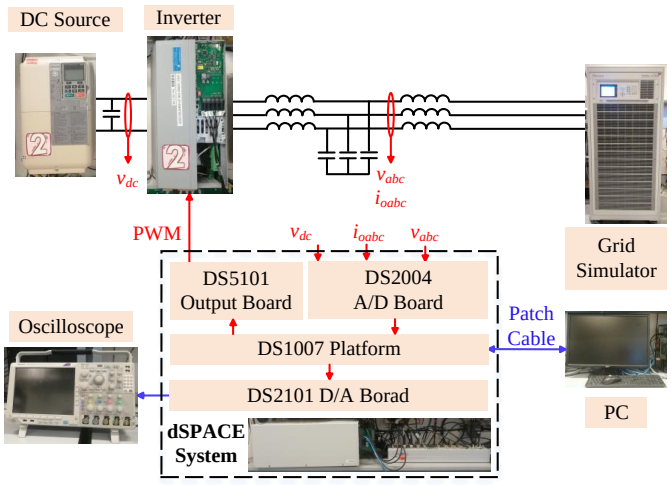

Fig. 8. Experimental configuration of MIMO-GFM converter.

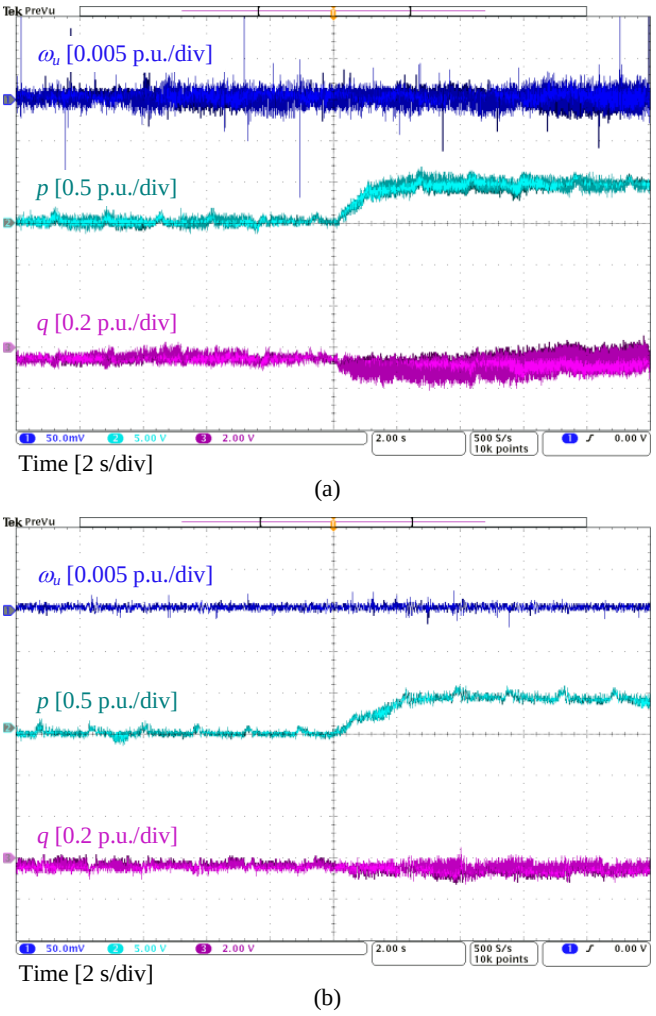

Fig. 9. Experimental comparison when P_{ref} steps from 0.5 p.u. to 1 p.u. (a) Original MIMO-GFM control. (b) Proposed MIMO-GFM control using direct state control.

and good low-frequency dynamics, the focused variables have large high-frequency components especially in the frequency ω_u. Therefore, as in the aforementioned discussion, pre-filters are necessary, where the corresponding waveforms can be found in [17]. In comparison, the proposed control can highly damp the high-frequency components without additional means.

A further comparison when ω_g decreases from 50 Hz to 49.9 Hz is shown in Fig. 10. Similar to Fig. 9, the proposed control can well damp the high-components, which is obviously observed with the original MIMO-GFM control. The results of Fig. 9 and 10 are in accordance with the theoretical analysis of Fig. 7.

B. System-Level Simulation Validation

This section study the system-level performance of the proposed method with disturbances from both inverter-side and system-side using the IEEE 9-Bus Test System shown in Fig. 11, where G3 is replaced by a VSC. The parameters are same as those in Table I and Table II in p.u. values. The average model of the inverter is used to improve the speed of the simulation. Therefore, the steady-state high-frequency components, which has been well shown in the experiments are neglected. The following disturbances are exerted to the system from the steady-state:

1) $t = 5$ s, a grid-side distubance is applied, where the output of G1 increases 0.1 p.u.;
2) $t = 10$ s, a inverter-side disturbance is applied, where P_{ref} of the VSC increases from 0.5 p.u. to 1 p.u.;
3) $t = 15$ s, a DC-side disturbance is applied, where V_{dcref} of the VSC increases from 1 p.u. to 1.01 p.u.;

Fig. 12 shows the simulation results using the IEEE 9-Bus Test System. It is observed that, in general, both the original MIMO-GFM (without and with pre-filters) and the proposed controls can guarantee the stable operation of the system responding to different disturbances. However, when a DC-side disturbance occurs, large high-frequency oscillations will be excited in the frequency and output powers of the inverter with original MIMO-GFM control. It has been explained from Fig. 2 that an error of $e_1 = V_{dcref} - v_{dc}$ will directly influence the frequency and internal voltage if there is not a pre-filter.

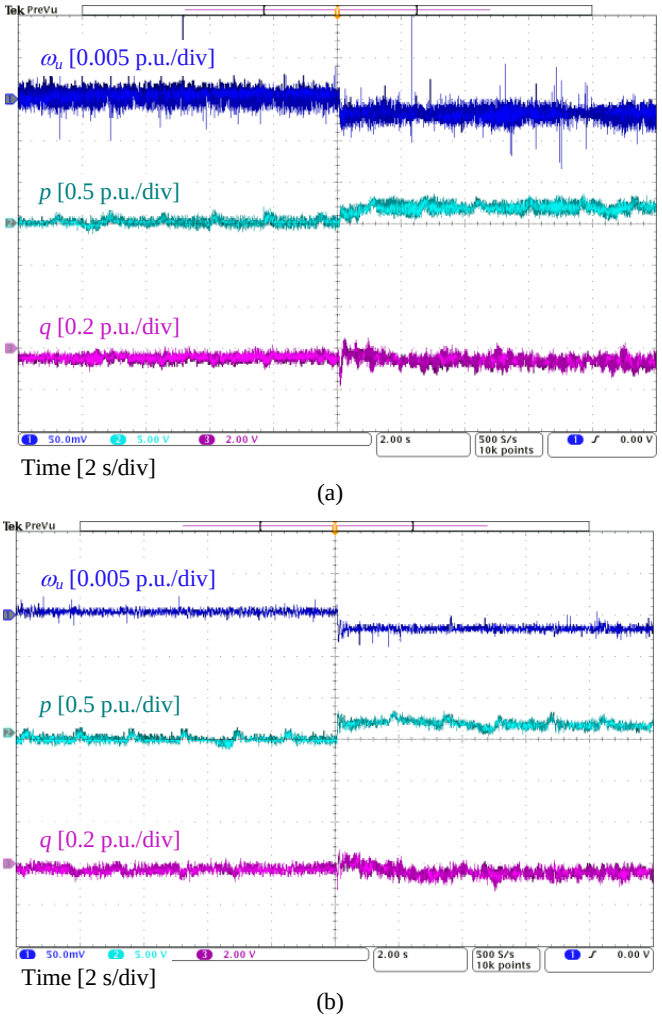

Fig. 10. Experimental comparison when ω_g decreases from 50 Hz to 49.9 Hz. (a) Original MIMO-GFM control. (b) Proposed MIMO-GFM control using direct state control

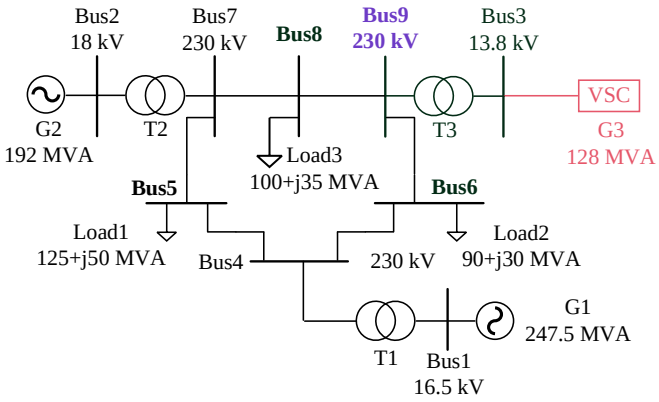

Fig. 11. Single-line diagram of IEEE 9-Bus Test System.

Such high-frequency oscillations can be suppressed if pre-filters are added. However, as the time constant of pre-filters increases, oscillations with low frequencies will occur as the pre-filters are not considered during the design of the original MIMO-GFM control. In comparison, the proposed MIMO-GFM control can well dampen such oscillations.

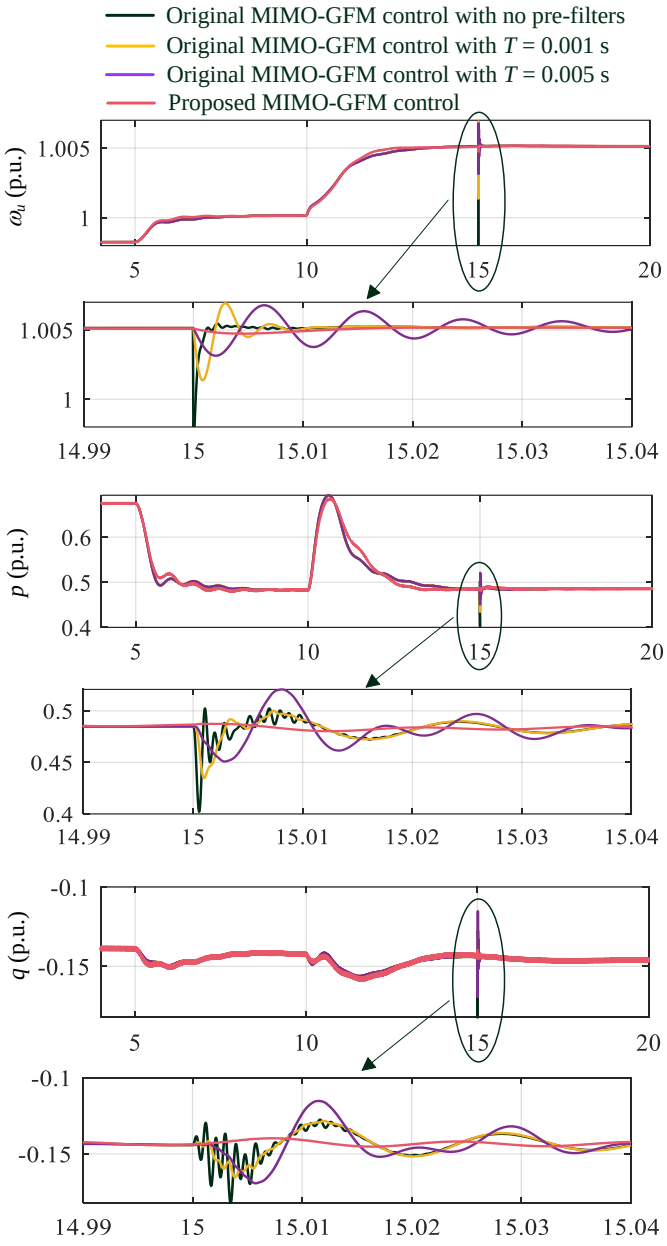

Fig. 12. Simulation results using IEEE 9-Bus Test System.

V. Conclusion

This paper proposes a novel control transfer matrix for the MIMO-GFM control. Instead of changing the states, the coupling terms of the proposed method only change the structure of the state differential equations and, at the same time, keep the frequency and voltage as the controlled states. By designing with the same $\mathcal{H}_\infty$ synthesis as the original MIMO-GFM control, the proposed method will have improved ability to decrease the impact of the high-frequency components on the system dynamics without increasing the complexity of the control system.

References

[1] M. Chen, D. Zhou, and F. Blaabjerg, "Multivariable grid-forming converters with direct states control," in *2022 IEEE Energy Convers. Congr. Expo. (ECCE)*, 2022, pp. 1–7.

[2] B. K. Bose, "Power electronics in smart grid and renewable energy systems," *Proc. IEEE*, vol. 105, no. 11, pp. 2011–2018, Nov. 2017.
[3] M. Eskandari and A. V. Savkin, "Robust PLL synchronization unit for grid-feeding converters in micro/weak grids," *IEEE Trans. Ind. Informatics*, vol. 19, no. 4, pp. 5400–5411, Apr. 2022.
[4] F. Deng, Y. Li, X. Li, W. Yao, X. Zhang, and P. Mattavelli, "A decentralized impedance reshaping strategy for balanced, unbalanced and harmonic power sharing in islanded resistive microgrids," *IEEE Trans. Sustain. Energy*, vol. 13, no. 2, pp. 743–754, Apr. 2022.
[5] J. Rocabert, A. Luna, F. Blaabjerg, and P. Rodríguez, "Control of power converters in AC microgrids," *IEEE Trans. Power Electron.*, vol. 27, no. 11, pp. 4734–4749, Nov. 2012.
[6] R. Rosso, X. Wang, M. Liserre, X. Lu, and S. Engelken, "Grid-forming converters: Control approaches, grid-synchronization, and future trends—a review," *IEEE Open J. Ind. Appl.*, vol. 2, pp. 93–109, Apr. 2021.
[7] M. Chen and X. Xiao, "Hierarchical frequency control strategy of hybrid droop/VSG-based islanded microgrids," *Electr. Power Syst. Res.*, vol. 155, pp. 131–143, Feb. 2018.
[8] N. Mohammed and M. Ciobotaru, "Adaptive power control strategy for smart droop-based grid-connected inverters," *IEEE Trans. Smart Grid*, vol. 13, no. 3, pp. 2075–2085, May 2022.
[9] H. Wu, X. Ruan, D. Yang, X. Chen, W. Zhao, Z. Lv, and Q.-C. Zhong, "Small-signal modeling and parameters design for virtual synchronous generators," *IEEE Trans. Ind. Electron.*, vol. 63, no. 7, pp. 4292–4303, Jul. 2016.
[10] J. Chen and T. O'Donnell, "Parameter constraints for virtual synchronous generator considering stability," *IEEE Trans. Power Syst.*, vol. 34, no. 3, pp. 2479–2481, May 2019.
[11] M. Chen, D. Zhou, C. Wu, and F. Blaabjerg, "Characteristics of parallel inverters applying virtual synchronous generator control," *IEEE Trans. Smart Grid*, vol. 12, no. 6, pp. 4690–4701, Nov. 2021.
[12] D. Pan, X. Wang, F. Liu, and R. Shi, "Transient stability of voltage-source converters with grid-forming control: A design-oriented study," *IEEE J. Emerg. Sel. Top. Power Electron.*, vol. 8, no. 2, pp. 1019–1033, Jun. 2020.
[13] C. Arghir, T. Jouini, and F. Dörfler, "Grid-forming control for power converters based on matching of synchronous machines," *Automatica*, vol. 95, pp. 273–282, Sep. 2018.
[14] J. Liu, Y. Miura, H. Bevrani, and T. Ise, "A unified modeling method of virtual synchronous generator for multi-operation-mode analyses," *IEEE J. Emerg. Sel. Top. Power Electron.*, vol. 9, no. 2, pp. 2394–2409, Apr. 2021.
[15] M. Chen, D. Zhou, and F. Blaabjerg, "Active power oscillation damping based on acceleration control in paralleled virtual synchronous generators system," *IEEE Trans. Power Electron.*, vol. 36, no. 8, pp. 9501–9510, Aug. 2021.
[16] L. Huang, H. Xin, and F. Dörfler, "$\mathcal{H}_\infty$-control of grid-connected converters: Design, objectives and decentralized stability certificates," *IEEE Trans. Smart Grid*, vol. 11, no. 5, pp. 3805–3816, Sep. 2020.
[17] M. Chen, D. Zhou, A. Tayyebi, E. Prieto-Araujo, F. Dörfler, and F. Blaabjerg, "Generalized multivariable grid-forming control design for power converters," *IEEE Trans. Smart Grid*, vol. 13, no. 4, pp. 2873–2885, Jul. 2022.
[18] H. Zhang, W. Xiang, W. Lin, and J. Wen, "Grid forming converters in renewable energy sources dominated power grid: Control strategy, stability, application, and challenges," *J. Mod. Power Syst. Clean Energy*, vol. 9, no. 6, pp. 1239–1256, Nov. 2021.
[19] A. Tayyebi, D. Gross, A. Anta, F. Kupzog, and F. Dörfler, "Frequency stability of synchronous machines and grid-forming power converters," *IEEE J. Emerg. Sel. Top. Power Electron.*, vol. 8, no. 2, pp. 1004–1018, Jun. 2020.
[20] Arani and El-Saadany, "Implementing virtual inertia in DFIG-based wind power generation," *IEEE Trans. Power Syst.*, vol. 28, no. 2, pp. 1373–1384, May 2013.
[21] J. Liu, Y. Miura, and T. Ise, "Comparison of dynamic characteristics between virtual synchronous generator and droop control in inverter-based distributed generators," *IEEE Trans. Power Electron.*, vol. 31, no. 5, pp. 3600–3611, May 2016.
[22] S. Dong and Y. C. Chen, "A method to directly compute synchronverter parameters for desired dynamic response," *IEEE Trans. Energy Convers.*, vol. 33, no. 2, pp. 814–825, Jun. 2018.

Meng Chen (Member, IEEE) received the B.Eng. degree in electrical engineering and automation from Qingdao University of Science and Technology, Qingdao, China, in 2013, the first Ph.D. degree in power system and automation from North China Electric Power University, Beijing, China, in 2018, and the second Ph.D. degree in energy technology from Aalborg University, Aalborg, Denmark, in 2022. He was an academic guest with Swiss Federal Institute of Technology (ETH) Zurich, Zurich, Switzerland, in 2021.

Since 2022, he was been with Aalborg University, where he is currently a Postdoctoral Researcher. His research interest is the control, stability, and reliability of power systems with power electronics. He is a recipient of the 2020 MPCE Best Paper Award.

Dao Zhou (Senior Member, IEEE) received the B.S. from Beijing Jiaotong University, Beijing, China, in 2007, the M. S. from Zhejiang University, Hangzhou, China, in 2010, and the Ph.D. from Aalborg University, Aalborg, Denmark, in 2014, all in electrical engineering.

Since 2014, he has been with Department of Energy Technology, Aalborg University, where currently he is an Associate Professor. His research interests include modeling, control, and reliability of power electronics in renewable energy applications. He serves as an Associate Editor for IET Renewable Power Generation and IET Power Electronics. He also received a few IEEE prized paper awards.

Frede Blaabjerg (Fellow, IEEE) was with ABB-Scandia, Randers, Denmark, from 1987 to 1988. From 1988 to 1992, he got the PhD degree in Electrical Engineering at Aalborg University in 1995. He became an Assistant Professor in 1992, an Associate Professor in 1996, and a Full Professor of power electronics and drives in 1998 at AAU Energy. From 2017 he became a Villum Investigator. He is honoris causa at University Politehnica Timisoara (UPT), Romania in 2017 and Tallinn Technical University (TTU), Estonia in 2018.

His current research interests include power electronics and its applications such as in wind turbines, PV systems, reliability, Power-2-X, power quality and adjustable speed drives. He has published more than 600 journal papers in the fields of power electronics and its applications. He is the co-author of eight monographs and editor of fourteen books in power electronics and its applications.

He has received 38 IEEE Prize Paper Awards, the IEEE PELS Distinguished Service Award in 2009, the EPE-PEMC Council Award in 2010, the IEEE William E. Newell Power Electronics Award 2014, the Villum Kann Rasmussen Research Award 2014, the Global Energy Prize in 2019 and the 2020 IEEE Edison Medal. He was the Editor-in-Chief of the IEEE TRANSACTIONS ON POWER ELECTRONICS from 2006 to 2012. He has been Distinguished Lecturer for the IEEE Power Electronics Society from 2005 to 2007 and for the IEEE Industry Applications Society from 2010 to 2011 as well as 2017 to 2018. In 2019-2020 he served as a President of IEEE Power Electronics Society. He has been Vice-President of the Danish Academy of Technical Sciences. He is nominated in 2014-2021 by Thomson Reuters to be between the most 250 cited researchers in Engineering in the world.